Research article

Enhanced adsorption of toluene on thermally activated ZIF-67: Characterization, performance, and modeling insights

Zabiholah Damiri [a], Saeed Jafari [a,*], Saeed Yousefinejad [a], Hossein Kazemian [b,c,d]

[a] Department of Occupational Health and Safety Engineering, School of Health, Shiraz University of Medical Sciences, Shiraz, Iran
[b] Materials Technology & Environmental Research (MATTER) Lab, University of Northern British Columbia, Prince George, BC, Canada
[c] Northern Analytical Lab Services (Northern BC's Environmental and Climate Solutions Innovation Hub), University of Northern British Columbia, Prince George, BC, Canada
[d] Environmental Sciences Program, Faculty of Environment, University of Northern British Columbia, Prince George, British Columbia, V2N4Z9, Canada

A B S T R A C T

The zeolitic imidazolate framework-67 (ZIF-67) has been explored for the dynamic adsorption of toluene vapor. We synthesized ZIF-67 through a straightforward room-temperature process and characterized it using XRD, FT-IR, DLS, and SEM techniques. The synthesized ZIF-67 possessed a Brunauer–Emmett–Teller (BET) surface area of 1578.7 m^2/g and 0.76 μm particle size. Thermal activation under various conditions revealed that ZIF-67, activated in dry air at 250 °C, demonstrated optimal adsorption efficacy. Its adsorption capacity, time of breakthrough, and time of equilibration were 414.5 mg/g, 420 min, and 795 min, respectively. We investigated the impact of diverse operational parameters on adsorption through breakthrough curve analysis. An increase in the toluene concentration from 100 to 1000 ppm enhanced the adsorption capacity from 171 to 414 mg/g, while breakthrough time decreased from 1260 min to 462 min, respectively.

Our findings show that increasing relative humidity from 0 to 70 % reduced 53.7 % in adsorption capacity and 46.3 % in breakthrough time. The competitive adsorption of toluene and ethylbenzene revealed that ZIF-67 had a higher selectivity for toluene adsorption. A 98 % adsorbent's regeneration efficiency at the first cycle reveals its reusability. The experimental data were successfully fitted to the Yan, Thomas, and Yoon-Nelson models to describe the adsorption process. The statistical validation of the model parameters confirms their reliability for estimating adsorption parameters, thus facilitating the design of fixed-bed adsorption columns for practical applications.

1. Introduction

The escalating air pollution problem is a pressing global issue, with the emission of Volatile Organic Compounds (VOCs) identified as a major contributor to indoor and outdoor air quality degradation [1]. VOCs originate primarily from anthropogenic activities and have been consistently released into the environment over the course of several decades [2]. Chemical process industries (CPI) are significant sources of VOCs, releasing compounds such as toluene, xylene, di-methyl chloride (DMC), methanol, and isopropyl alcohol

---

during the handling, storage, and distribution of various chemicals [3]. The environmental impact of these VOCs is profound, adversely affecting human health and contributing to atmospheric changes that lead to issues like the greenhouse effect, photo-chemical smog, and stratospheric ozone depletion [4]. Additionally, the interaction between atmospheric nitrogen oxides (NOx) and VOCs plays a key role in forming tropospheric ozone, a critical pollutant [3,5].

The subgroup of VOCs known as BTEX (benzene, toluene, ethylbenzene, and m/p/o-xylene) is especially prevalent in emissions and is derived from petroleum products and industrial solvents used in the manufacture of paints, rubber, and adhesives [6–8]. These compounds have been designated as hazardous air pollutants (HAPs) by the US EPA [7] and the International Agency for Research on Cancer (IARC) has categorized them according to their carcinogenicity [7].

To mitigate VOC emissions, control techniques are deployed, which are bifurcated into destruction and recovery methods [9]. Destruction methods aim to decompose VOCs into harmless or less harmful compounds, whereas recovery methods, like adsorption, focus on reclaiming valuable VOCs and reducing carbon emissions [7]. Among these, adsorption stands out for its high efficiency, cost-effectiveness, and low energy consumption, making it a favorable option for VOC abatement, particularly at low concentrations [10].

Adsorption relies on the specific surface area (SSA) of materials, which is indicative of the availability of active adsorption sites and is a key factor in adsorptive performance [11]. Additionally, pore size distribution and surface functionality also play significant roles. Various materials, including activated carbon, zeolites, and metal-organic frameworks (MOFs), have been employed as VOC adsor-bents [7].

MOFs, in particular, offer a unique combination of metal ion clusters and organic linkers that form highly porous structures, leading to materials with exceptional SSA and chemical functionality [12]. These characteristics and thermal and chemical stability have made MOFs a focal point in research and practical applications [13–15]. The exceptional properties of MOFs have attracted considerable attention in recent years for their application as adsorbents for organic and inorganic contaminants in aquatic environments [16–19].

Recent advancements in VOC adsorption techniques have seen significant contributions from researchers exploring the efficacy of metal-organic frameworks. Notably, studies have highlighted using MOF-199-based coatings on solid-phase microextraction (SPME) fibers to enhance the capture and analysis of VOCs from air samples. This innovative approach leverages the high surface area and selectivity of MOF-199 for efficient sampling and pre-concentration, as detailed in the 2023 study [20]. A 2021 publication introduced a novel in situ solvothermal synthesis of MOF-199 coatings on SPME fibers, marking an improvement in the robustness and adsorption performance of the fibers [21].

Furthermore, a comprehensive review in 2022 outlined the various preparation methods and diverse applications of MOF-based SPME coatings, affirming their effectiveness across a spectrum of VOCs. These studies collectively underscore the potential of MOFs as a transformative technology in environmental monitoring and highlight the ongoing evolution of methods for pollution control [22].

Zeolitic imidazolate frameworks (ZIFs) stand out within the MOF family due to their zeolite-like structures and MOF properties, offering high surface areas and stability [23–27]. ZIF-67, a cobalt-based ZIF with a sodalite topology, has demonstrated a significant adsorption potential, with a high SSA and an array of active sites for molecular adsorption [26,28].

Although ZIF-67 has been studied for removing pollutants from aqueous solutions [28–30], its application for adsorbing VOCs from air is less explored. Noteworthy studies include the work by H.S. Jhinjer et al. on ZIF-67 functionalized fabrics [31], Vellingiri et al.'s toluene adsorption capacity study [32], and Bian et al.'s formaldehyde removal investigation [33].

The efficiency of adsorption processes, particularly in fixed-bed columns, is often assessed by analyzing breakthrough curves, which provide crucial data for determining the operational parameters of adsorption systems [34–36]. The adsorption and removal of toluene from high-concentration air phases holds immense environmental and health implications. Researchers in this field are eagerly seeking any ideas that could contribute to resolving this issue. The identification of innovative materials for toluene absorption, filtration, removal, and decomposition can be considered a proactive measure towards regulating its concentration. It is essential to investigate and determine the adsorption capacity of toluene on the adsorbing materials to demonstrate the efficacy of these materials in reducing pollutant concentration and minimizing their impact on human health. Activated carbo [37], Zeolite [38], ZIF-8 [39], UiO-66(NH2) [40], UiO-66 [41], MIL-101(Fe), MOF-5 [32], and MOF-177 [42] have been investigated as toluene adsorbents, but the adsorption behavior of ZIF-67 as a toluene adsorbent has yet to be investigated.

This study specifically focuses on the application of ZIF-67 in toluene adsorption. Furthermore, this study presents a comprehensive examination of the characterization, performance, and modeling insights regarding the process of toluene adsorption. The method-ology section includes the preparation and thermal activation of ZIF-67, followed by investigations of its structural, morphological, and surface properties. Therefore, this study aims to extend the application domain of ZIF-67 to the gas phase by evaluating its effectiveness in a fixed-bed column setup for toluene removal.

2. Material and methods

2.1. Sample preparation

Cobalt nitrate hexahydrate (Co (NO₃)₂·6H₂O 99.9 %), 2-Methylimidazole (C4H6N2 99 %), Methanol (CH3OH) and Ethanol (C2H5OH) were supplied from Sigma Aldrich. All the aforementioned materials were of analytical grade and were used without any additional treatment.

A two-solution approach was adopted for the synthesis of ZIF-67. Initially, 1.65 g of 2-methylimidazole was dissolved in a 100-mL solvent mixture of methanol and water (1:1 v/v) with continuous stirring to form the organic ligand solution. Separately, the metal

solution was prepared by dissolving 0.7 g of cobalt nitrate hexahydrate in the same solvent mixture. The metal solution was then gradually introduced to the ligand solution, stirring for 10 min at room temperature and atmospheric pressure. The reaction mixture was left to age at room temperature for 24 h, forming purple-colored precipitates, which were harvested by centrifugation at 8000 rpm for 10 min. The centrifuged product underwent quintuple washing with 60 mL of absolute ethanol and subsequent centrifugation. The final product was then oven-dried at 60 °C for an extended period [43].

2.2. Characterization

X-ray diffraction (XRD) analysis was performed to ascertain the crystal structure and purity of the ZIF-67 samples. A D8 Advance (Bruker, Germany) diffractometer equipped with Cu Kα radiation was utilized, scanning between 5° and 40° 2θ at a rate of 2° per minute and a step increment of 0.02°. Fourier transform infrared (FTIR) spectroscopy was conducted on a PerkinElmer-Spectrum RXI (PerkinElmer, USA) to record the vibrational spectra across a range of 4000–400 cm^{-1}.

Scanning electron microscopy (SEM) provided insights into the size and morphology of the synthesized particles. A CamScan MV 2300 (CamScan, Canada) operated at 20 kV was employed, and samples were prepared on conductive adhesive tape with a sputtered gold layer to minimize charging effects.

Particle size distribution was determined through Dynamic Light Scattering (DLS) using a Horiba LB-550 (Horiba, Japan). The surface areas and pore volume were evaluated via nitrogen adsorption-desorption isotherms using a Belsorp Mini II (MicrotracBEL, Japan). The standard Brunauer-Emmett-Teller (BET) equation derived the surface area, while the mesopore and micropore volumes were calculated using the BJH and t-plot methods. Samples were degassed at 150 °C for 3 h under vacuum conditions before the adsorption measurements.

2.3. Experimental setup

The evaluation of ZIF-67's dynamic adsorption behavior was performed in a fixed bed column apparatus under atmospheric pressure. The gas-phase toluene was generated via a controlled injection method. High-purity toluene (Merck, 99.99 %) was introduced into a stream of nitrogen gas (99.999 %) to create a calibrated gaseous toluene mixture. A syringe pump (Chemyx Fusion 100, USA) precisely controlled the toluene injection rate, while the nitrogen flow was regulated by a mass flow controller (Alicat MC-Series, USA). This mixture was then allowed to equilibrate within a 25-mL mixing chamber before being introduced to the column.

The adsorption column, a quartz tube of 15 cm in length and 0.2 cm in internal diameter, was packed with a predetermined amount of ZIF-67 and glass wool. Gas chromatography coupled with a flame ionization detector (GC-FID, Varian CP 3800) was utilized to monitor the toluene concentration at the inlet and outlet of the column. The setup of the experimental apparatus is depicted in Fig. 1.
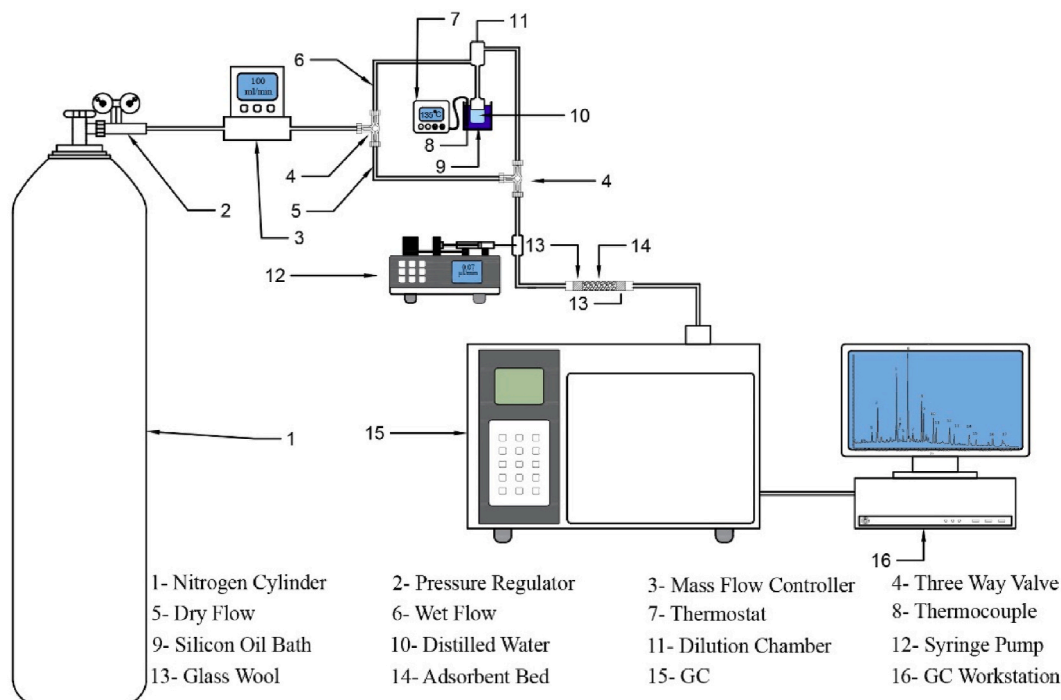

1- Nitrogen Cylinder	2- Pressure Regulator	3- Mass Flow Controller	4- Three Way Valve
5- Dry Flow	6- Wet Flow	7- Thermostat	8- Thermocouple
9- Silicon Oil Bath	10- Distilled Water	11- Dilution Chamber	12- Syringe Pump
13- Glass Wool	14- Adsorbent Bed	15- GC	16- GC Workstation

Fig. 1. Schematic diagram of the continuous flow fixed bed reactor for toluene dynamic adsorption by ZIF-67.

2.4. Adsorption parameters

The adsorption efficiency of ZIF-67 was determined by analyzing the breakthrough curves, which plot the relative concentration of toluene vapor at the column's inlet (C_0) and outlet (C) over time. The experimental conditions were meticulously controlled, including the toluene concentration in the feed and the flow rates of the toluene injection (Q_p, μL/hr) and the nitrogen diluent (Q_d, L/min). These parameters were set to pass through the column containing a known mass of ZIF-67 (mg). Breakthrough time (t_b, min) and time to reach adsorption equilibrium (t_e, min) were identified when the outlet concentration ratios reached 0.1 and 0.95, respectively, as shown in Fig. 2(a).

The adsorption capacity (q, mg/g) was calculated by measuring the mass of toluene adsorbed (m_a) per unit mass of adsorbent during t_e, derived as follows:

$$q = \frac{Q_d c_0}{m}\left(t_e - \frac{1}{c_0}\int_0^{t_e} c \cdot d_t\right) \tag{1}$$

This equation [1] infers that the adsorption capacity is proportional to the area under the breakthrough curve, representing the concentration of adsorbed toluene ($C_{ads} = C_0 - C$) over time t_e, normalized by the mass of the adsorbent. The graphical representation of the adsorption capacity is the area below the breakthrough curve up to the time t_e, as shown in Fig. 2 [44–46].

2.5. Thermal pretreatment of adsorbents

The influence of thermal pretreatment on ZIF-67's adsorption capabilities was evaluated under various temperatures and atmospheric conditions. For each trial, a 0.1 g sample of ZIF-67 was placed inside a quartz tube. A continuous flow of either dry air or pure nitrogen at 0.02 L/min was then introduced through the tube. The samples were incrementally heated to target temperatures of 200 °C, 250 °C, and 300 °C in an air environment and 300 °C and 400 °C under a nitrogen atmosphere. These samples were denoted as ZIF-67$_{air}$/200 °C, ZIF-67$_{air}$/250 °C, ZIF-67$_{air}$/300 °C, ZIF-67$_{N2}$/300 °C, and ZIF-67$_{N2}$/400 °C, respectively. Post-heating, the samples were allowed to return to room temperature before their adsorption properties were assessed.

2.6. The effect of relative humidity (RH) on adsorption performance

To explore the impact of relative humidity on ZIF-67's adsorption performance, RH was manipulated using an evaporation technique. The carrier gas was passed over distilled water maintained at a fixed temperature, thus generating water vapor at a consistent rate. A PID-regulated silicone oil bath controlled the temperature around a flask containing 20 mL of distilled water to attain target RH levels (40 %, 60 %, and 80 %) in the effluent carrier gas. Toluene vapor was introduced into this humidified stream and channeled through the pre-treated adsorbent bed to measure adsorption efficacy.
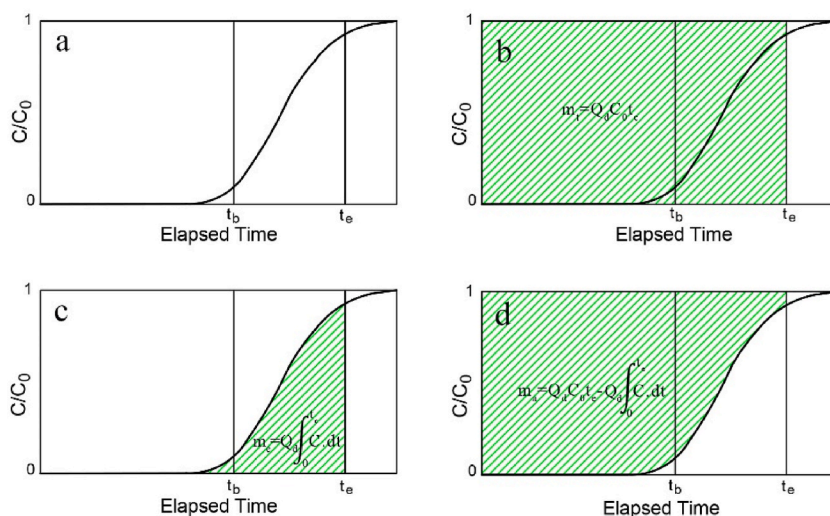

Fig. 2. Determination of the adsorption parameters using the breakthrough curves (a) schematic of a breakthrough curve indicating the breakthrough time t_b and the equilibrium time t_e. (b) The surface indicating the complete mass of adsorbate in the influent gas m_t during t_e (c) the surface indicating the complete mass of adsorbate in the effluent stream m_e during t_e (d) the surface indicating the complete mass of adsorbate taken up during t_e.

2.7. Mathematical modeling

In the design of adsorption column systems, accurately estimating parameters such as breakthrough time and adsorption capacity is vital. Traditional experimental methods to evaluate these factors are often complex and resource-intensive. Alternatively, mathematical modeling provides a feasible approach to predict adsorption behaviors. This study applied the Yoon-Nelson [47], Yan, and Thomas models [48,49], which are recognized for their simplicity and lack of need for extensive adsorbent and adsorbate details or the physical dimensions of the adsorption bed.

The mathematical expressions for the Yoon-Nelson, Yan, and Thomas models are as follows:

$$t = \tau + \frac{1}{k'} ln \frac{C}{C_0 - C} \tag{3}$$

$$\frac{C}{C_0} = 1 - \frac{1}{1 + \left(\frac{C_0 Q t}{q_y m}\right)^{A_y}} \tag{4}$$

$$\frac{C}{C_0} = \frac{1}{1 - exp\left(\frac{K_T q_T m}{Q} - K_T C_0 t\right)} \tag{5}$$

here, C and C_0 represent the concentrations of the adsorbate in the effluent and influent (mg/mL), respectively; t is the operational time (min); τ is the time when C/C_0 reaches 50 % (min); k' is the Yoon-Nelson rate constant (min^{-1}); m is the adsorbent mass (g); Q is the flow rate of the carrier gas (mL/min); A_y and K_t are constants for the Yan and Thomas models, respectively; and q_y and q_T are the estimated adsorption capacities (mg/g) by the Yan and Thomas models, respectively.

3. Results and discussion

3.1. Characterization

The crystalline integrity and structural purity of ZIF-67 were determined using X-ray diffraction (XRD), as depicted in Fig. 3. The XRD patterns displayed distinct peaks at specific 2θ values (7.35°, 10.40°, 12.75°, 14.73°, 16.48°, 22.18°, and 24.55°), congruent with the simulated patterns of sodalite structures [28,50,51], confirming the formation of ZIF-67.

Fourier-transform infrared spectroscopy (FTIR) further elucidated the surface chemical interactions and bonding within the synthesized ZIF-67, as shown in Fig. 3. Peaks corresponding to the 2-methylimidazole ligands matched previously reported spectra for ZIF-67. The IR bands within the 600–1500 cm^{-1} region indicate the imidazole ring's bending and stretching vibrations, while the band at 1584 cm^{-1} is linked to the C=N bond stretch in 2-methylimidazole [50]. The peaks at 2929 and 3135 cm^{-1} arise from the C–H and N–H stretching vibrations, respectively [52], and the band at 431 cm^{-1} is associated with the Co–N stretch [50].

The specific surface area and porosity characteristics of ZIF-67 were assessed through nitrogen gas adsorption-desorption isotherms at 77 K, as presented in Fig. 4. The resulting isotherms are of type I, typical for microporous materials, with a BET surface area of 1578.7 m^2/g and a total pore volume of 0.6 cm^3/g.

Scanning electron microscopy (SEM) provided insights into the morphology of ZIF-67, as shown in Fig. 5. The SEM images revealed uniformly shaped particles with rhombic dodecahedral forms. The particles measured in the micrometer range, with an average diameter of approximately 2 μm and edge lengths around 700 nm.

Dynamic light scattering (DLS) was employed to determine the particle size distribution of ZIF-67, with the results displayed in a
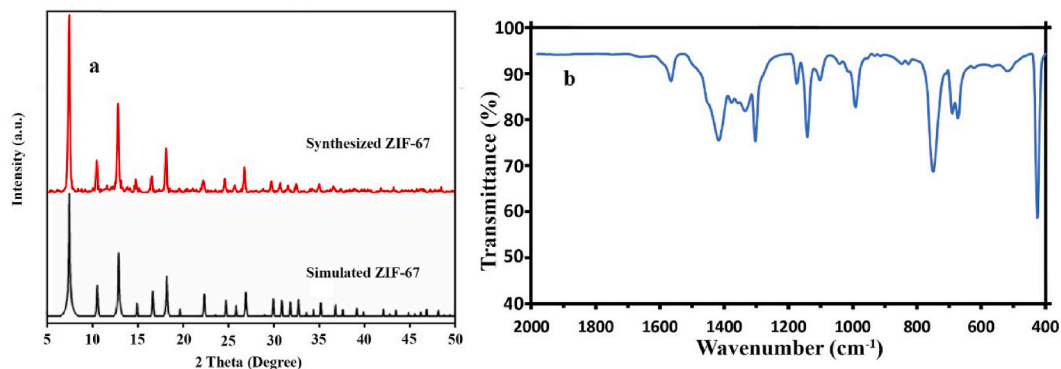

Fig. 3. As-synthesized and simulated XRD patterns of ZIF-67 (a) and FTIR spectra of the as-synthesized ZIF-67 (b).
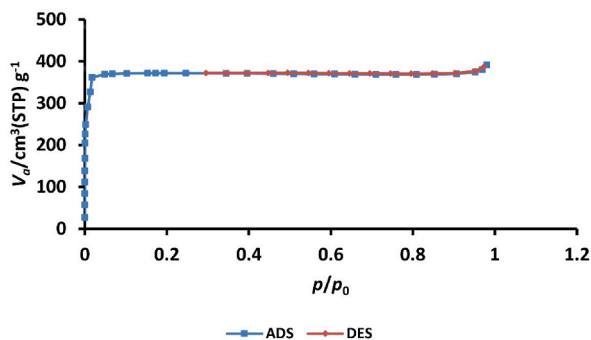
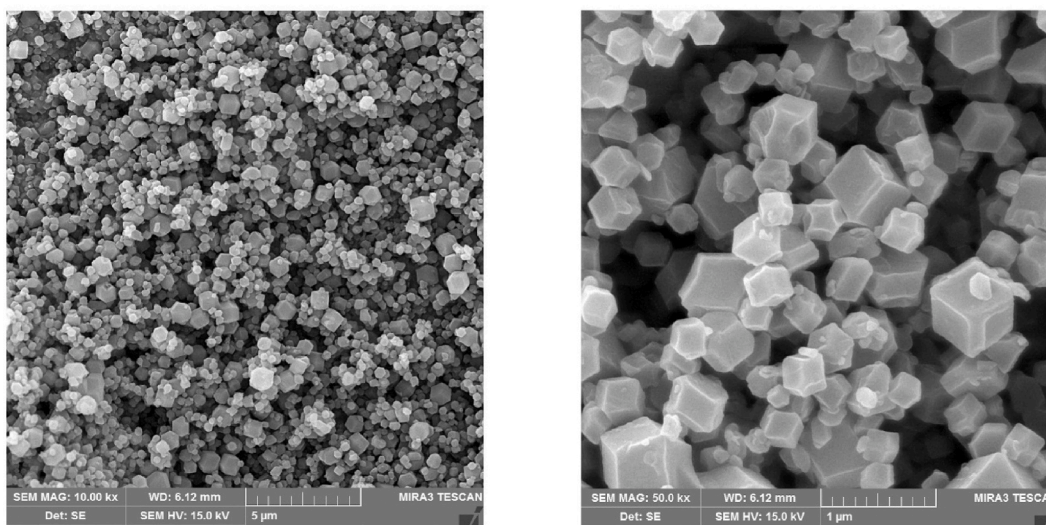**Fig. 4.** Nitrogen adsorption–desorption isotherms of the as-synthesized ZIF-67.

Fig. 5. SEM micrographs of ZIF-67 at (a) 10000 and (b) 50000 magnifications.

histogram in Fig. 6. The synthesis method yielded a range of particle sizes from 247 nm to 3.205 μm, with an average particle diameter of 760.7 (±493.1) nm and a predominant distribution between 400 and 600 nm.

3.2. Activation

Activating as-synthesized MOF materials is imperative to remove entrapped guest molecules such as solvents, unreacted linkers or cluster precursors, and modulators, thereby revealing the intrinsic porous structure for application purposes. Achieving the optimal surface area and pore volume without compromising the MOF's structural integrity requires careful activation methods tailored to the interactions between the guest molecules and the MOF framework. Activation procedures commonly include thermal treatments, akin to those used for carbon and zeolite adsorbents [53–56].

As detailed earlier, our study utilized a range of temperatures and atmospheres for pre-treatment, followed by an assessment of the dynamic adsorption parameters of the cooled samples (Table 1). These parameters were derived from the toluene adsorption
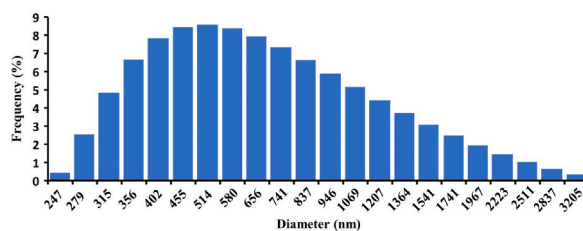

Fig. 6. Particle size distributions of as-synthesized ZIF-67 sample from DLS examination.

Table 1
Dynamic adsorption parameters of ZIF-67 for toluene adsorption pretreated at various conditions.

Adsorbents	adsorption capacities (mg/g)	breakthrough time (min)	equilibrium time (min)	Total adsorption percentage	LUB value (cm)
As-synthesis ZIF-67	31.6	0	180	21.1	4
ZIF-67$_{Air}$/200 °C	148.1	0	270	66.6	4
ZIF-67$_{Air}$/250 °C	414.5	420	795	77.7	1.88
ZIF-67 $_{Air}$/300 °C	160.1	0	330	61.3	0
ZIF-67 $_{N2}$/300 °C	82.6	0	210	53.6	0
ZIF-67$_{N2}$/400 °C	258.7	225	375	33.5	1.6

breakthrough curves for ZIF-67 post-activation.

The breakthrough adsorption efficiency of ZIF-67 was evaluated using a continuous flow, fixed-bed reactor at atmospheric pressure. For a standard adsorption test, 0.1 g of the thermally pretreated ZIF-67 was packed into a quartz tube, through which a carrier gas stream containing 1000 ppmv of toluene was passed at 0.02 L/min at ambient temperature. Breakthrough curves, which plot the normalized concentration (C/C_0) against time, elucidate the adsorption performance of ZIF-67 subjected to different activation temperatures under air and nitrogen atmospheres, as depicted in Fig. 7(a) and (b). Notably, the adsorption efficiency of ZIF-67$_{Air}$ samples initially increases with pretreatment temperature up to 250 °C and then diminishes at 300 °C (Fig. 7(a)). Conversely, ZIF-67$_{N2}$ samples show a marked improvement in adsorption efficiency with an increase in pretreatment temperature from 300 °C to 400 °C (Fig. 7(b)).

Dynamic adsorption parameters are determined from the breakthrough curves, and the derived calculations are summarized in Table 1. The adsorption capacities for ZIF-67$_{Air}$/250 °C and ZIF-67$_{N2}$/300 °C were 414.5 mg/g and 258.7 mg/g, respectively. The breakthrough occurred at 420 min for ZIF-67$_{Air}$/250 °C and 225 min for ZIF-67$_{N2}$/300 °C, with adsorption equilibrium reaching 795 min and 375 min, respectively.

Thermogravimetric analyses (TGA) in previous investigations have established the thermal resilience of ZIF-67, identifying weight losses around 350 °C possibly due to the release of entrapped molecules or unreacted species. Remarkably, ZIF-67 maintains structural integrity up to approximately 500 °C before framework collapse, a threshold that surpasses many other MOF materials [28,43,57,58].

The adsorption efficacy is influenced by the interplay between the adsorbate and adsorbent, with the adsorbate's polarizability being a pivotal factor. X. Wang and colleagues estimated the binding energy of toluene to the adsorbent, revealing a predominant π-π stacking interaction [1].

MOFs, with their metal clusters and organic linkers, exhibit a blend of lipophilic traits [59,60]. Within the ZIF framework, 2-methylimidazole imparts a hydrophobic nature that facilitates the adsorption of organic molecules [60]. Specifically, aromatic VOCs like toluene adsorption onto ZIF-67 is attributed to π-π interactions between toluene molecules and 2-methylimidazolate linkers. These interactions are stronger than other interactions such as O-π and C-π found in VOC adsorption with zeolites and activated carbon [39, 59].

Table 2 compares the toluene adsorption capacities of ZIF-67 with other adsorbents. According to the data presented, ZIF-67 exhibits higher toluene adsorption capacities than ZIF-8, zeolites, silica gel, and activated carbons.

3.3. Impact of humidity on dynamic adsorption

Fig. 8 illustrates the toluene breakthrough curves on ZIF-67$_{Air}$/250 °C under varying relative humidity (RH) levels of 30 %, 50 %, and 70 %. Dynamic adsorption parameters, deduced from these curves, are detailed in Table 3. It was observed that an increase in RH from 0 % to 70 % led to a substantial decrease in the adsorption characteristics of toluene, with reductions in adsorption capacity, breakthrough time, and equilibrium time by approximately 53.7 %, 46.3 %, and 52.8 %, respectively.

The synthesis process of ZIF-67 inherently concludes with neutral imidazolate ligands coordinating with metal atoms (such as Co) by donating their electron pairs to maintain charge neutrality. This coordination confers -N-H functional groups on the ZIF surfaces,
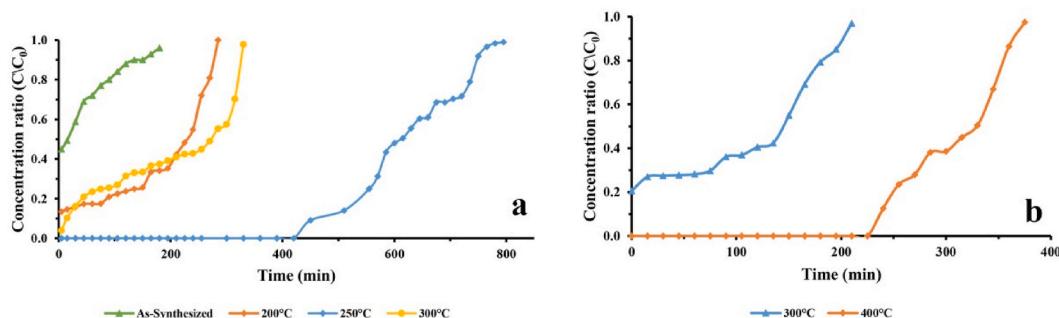

Fig. 7. Breakthrough curves of toluene adsorption on ZIF-67 (a) after pretreatment in dry air at 200 °C, 250 °C, 300 °C, and as-synthesized sample and (b) after pretreatment in nitrogen atmosphere at 200 °C and 300 °C.

Table 2
Comparison of the adsorption capacities of ZIF-67 and some other adsorbents for toluene.

| Adsorbents	Q (mg/g)	Surface Aria BET (M^2/g)	Adsorption models	Reference
ZIF-67	414.5	1578.7	Dynamic adsorption	Present study
Carbonized- polydopamine (C-PDA)	1254.9	3291	Static adsorption	[1]
ZIF-8	381.5	1305	Dynamic adsorption	[39]
MOF-177	585	2970	Static adsorption	[42]
Zeolite L	99.51	322	Static adsorption	[38]
Activated carbon	176.91	1339	Static adsorption	[37]
Cu-BTC@GO	259.83	1362.7	Static adsorption	[61]
Silica gel	205	765.6	Dynamic adsorption	[62]
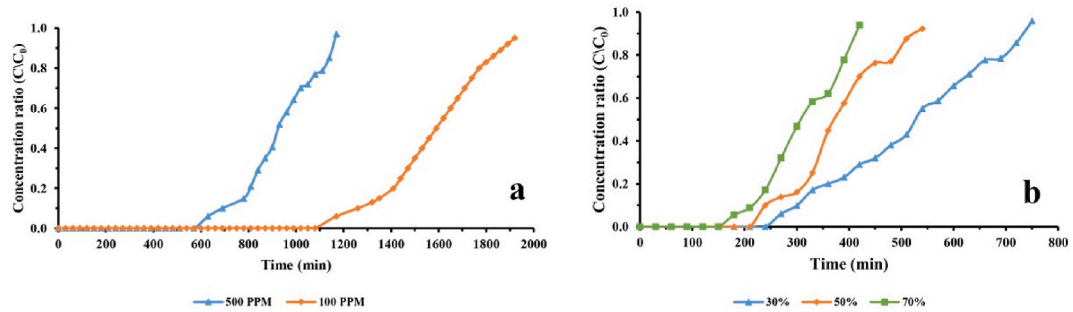
Fig. 8. Effect of operating parameters on breakthrough curves of toluene adsorption on ZIF-67 at (a) different concentrations and (b) different relative humidity.

Table 3
Dynamic adsorption parameters of ZIF-67 for toluene adsorption at various relative humidity and concentrations.

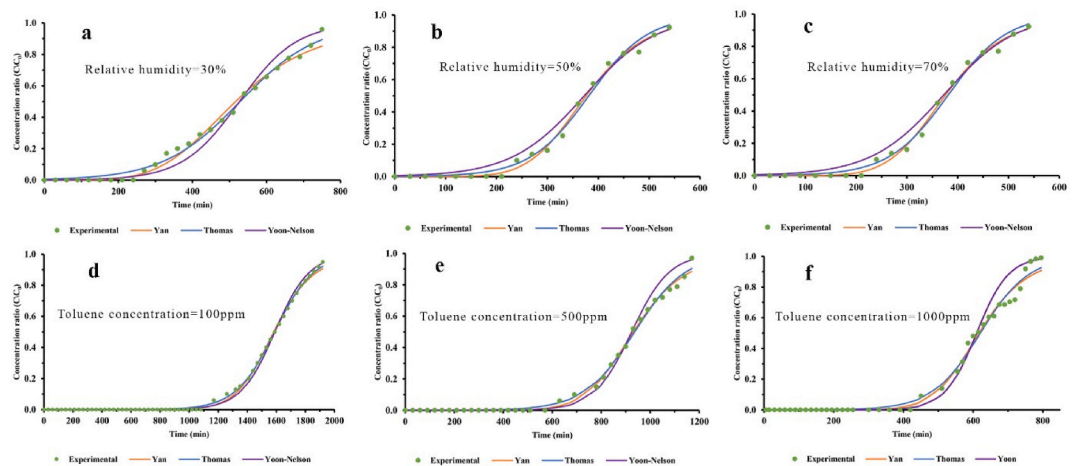| Operating parameters		adsorption capacities (mg/g)	breakthrough time (min)	equilibrium time (min)	Total adsorption percentage (%)	LUB value
Relative humidity (%)	30	353.8	300	750	62.2	2.4
	50	271.4	240	540	70.5	2.22
	70	222.5	214	420	74.3	1.96
Toluene concentration (ppm)	100	171.5	1260	1920	80.7	1.38
	500	381.9	690	1170	79.2	1.64
	1000	414.5	462	795	77.7	1.68

Fig. 9. Estimated breakthrough curves of toluene adsorption on ZIF-67$_{Air}$/250 °C at various operating conditions with Yan, Thomas, and Yoon-Nelson models.

which are prone to hydrogen bonding with water vapor, leading to a monolayer of water on the ZIF surfaces. The FT-IR spectra further corroborate this, where the absorption band at 3418 cm^{-1} is indicative of hydrogen-bonded N–H stretching (Fig. 3(b)) [52]. At elevated humidity levels, water molecules preferentially adsorb on the external surfaces of ZIF-67, thereby hindering toluene adsorption within its internal pore structure.

3.4. Impact of toluene concentration on dynamic adsorption

The dynamic adsorption process is also affected by the concentration of toluene in the influent gas, as depicted in Fig. 8(b). ZIF-67$_{Air}$/250 °C exhibited adsorption capacities of 171.5 mg/g and 381.9 mg/g at toluene concentrations of 100 ppmv and 500 ppmv, respectively, with corresponding breakthrough times of 1080 and 570 min. Consequently, an increased toluene concentration enhances the mass transfer rate to ZIF-67$_{Air}$/250 °C.

3.5. Mathematical modeling

The adsorption behavior of toluene on ZIF-8$_{Air}$/250 °C under various conditions was mathematically simulated using the Yan, Thomas, and Yoon-Nelson models through non-linear regression, and the findings are presented in Fig. 9(a–f). The statistical parameters of the model fits are summarized in Table 3.

The correlation coefficients (R^2) for the Yan, Thomas, and Yoon-Nelson models range from 0.998 to 0.989, 0.999 to 0.989, and 0.985 to 0.75, respectively, indicating a strong alignment of the experimental data with the proposed models.

The estimated adsorption capacities (q_y and q_T) from the Yan and Thomas models align closely with the experimentally determined capacities, as indicated by the comparison in Table 4. These values suggest that the models can reliably approximate the empirical data.

Breakthrough times deduced from the models (Table 4) align well with the experimental data and do not exhibit significant deviations.

These models have demonstrated their utility in predicting the dynamic adsorption parameters, thereby facilitating the design and optimization of fixed-bed column adsorption systems for practical applications.

3.6. Adsorption- desorption cycle

In order to enhance the economic viability and attractiveness of the adsorption process for industrial applications, it is imperative to assess the reusability of the spent (saturated) adsorbent following regeneration [63]. The regeneration process not only facilitates the recovery of the saturated adsorbent for reuse, but also enables the extraction of a highly concentrated adsorbate as a value-added product. Consequently, the regeneration of the adsorbent is pivotal in reducing the operational expenses associated with pollution control systems. To ensure an effective regeneration of the adsorbent, the regeneration process must minimally impact its performance [64]. ZIF-67 regeneration process was down at 200 °C and a 200 mL/min nitrogen flow rate. The effluent's toluene concentration was determined, and the regeneration efficiency was computed using the subsequent equation [64].

$$E\ (\%) = \frac{m_r}{m_a} * 100 \tag{6}$$

in this equation, m_r is the mass of toluene desorbed (mg) during regeneration time, and m_a is the mass of toluene adsorbed (mg) at equilibrium time (t_e). Fig. 10 displays the regeneration experiment curves of ZIF-67 at a temperature of 200 °C.

The ZIF-67`s regeneration efficiency was 98 %, which reveals that toluene was successfully recovered and that the ZIF-67 can be reusable. This high regeneration efficiency evidences that the primary mechanism responsible for toluene adsorption is physisorption.

3.7. Competitive adsorption of toluene and ethylbenzene on ZIF-67

The competitive adsorption of a mixture of toluene and ethylbenzene vapor was examined at a flow rate of 200 mL/min and a concentration of 200 ppm for both analytes. Table 5 presents the adsorption parameters for both toluene and ethylbenzene.

Fig. 11 shows the breakthrough curves for toluene and ethylbenzene adsorption. The adsorption capacity for toluene was 218 mg/g, while for ethylbenzene it was 143 mg/g.

Competitive absorption occurs as a result of the co-presence of VOC mixtures in the absorption process. VOCs with higher affinities displace those with lower affinities. Several factors influence this process, including VOC polarity, molecular weight, and boiling point. VOCs with higher boiling points and molecular weights have a greater tendency to occupy adsorption sites [65,66]. ZIF-67 is a hydrophobic and non-polar adsorbent that can adsorb non-polar compounds under competitive conditions. Therefore, toluene and ethylbenzene compete in adsorption due to their non-polar properties. The results show that toluene has a higher adsorption capacity in competitive adsorption, which can be attributed to its smaller size compared to ethylbenzene.

The ZIF-67 adsorbent is highly effective in absorbing various chemical compounds, including toluene. It offers several notable advantages that make it an exceptional choice for this purpose. By incorporating the ZIF-67 adsorbent into the design of an adsorption bed, it becomes possible to prevent the release of VOCs such as toluene into the environment. Toluene is known to have significant adverse effects on human health, particularly in the airborne phase.

Table 4

Comparison of statistical and adsorption parameters of the Yan, Thomas, and Yoon-Nelson models resulting from the fitting of experimental toluene breakthrough curves adsorption on ZIF-67$_{Air}$/250 °C.

| Model	Parameters	Relative Humidity (%)			Toluene Concentration (ppm)		
		30	50	70	100	500	1000
Yan	A_y	4.7	6.4	5.82	11.77	8.96	9
	q_y	367.7	267.9	221.7	174.1	383.7	414.8
	R^2	0.989	0.994	0.989	0.998	0.995	0.989
	t_b	322	296	212	1320	720	478
Thomas	K_t	2.7	4.85	5.44	13.52	4.66	4.3
	q_t	376.4	271.6	225.3	174.7	385.9	417.2
	R^2	0.992	0.991	0.988	0.999	0.995	0.989
	t_b	300	282	200	1290	703	464
Yoon-Nelson	k'	0.013	0.014	0.023	0.0085	0.013	0.022
	R^2	0.822	0.985	0.922	0.973	0.75	0.84
	t_b	357	244	212	1330.8	746	510
Experimental	q	353.8	271.4	222.5	171.5	381.9	414.5
	t_b	300	240	214	1260	690	462
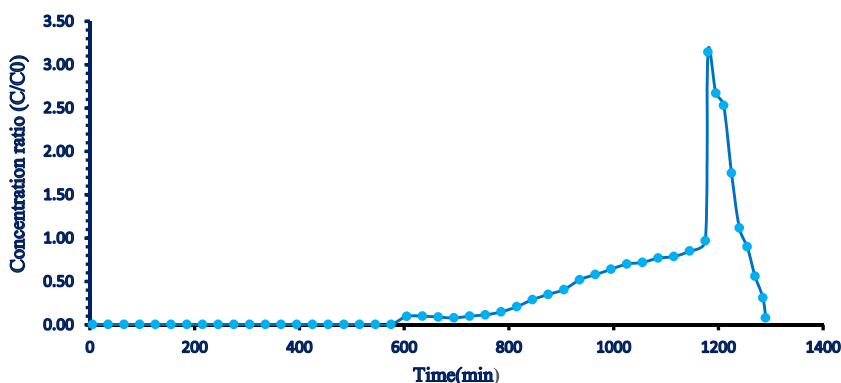
Fig. 10. Regeneration curves of ZIF-67 at 200 °C.

Table 5

Comparative adsorption parameters of ZIF-67 for toluene and ethylbenzene.

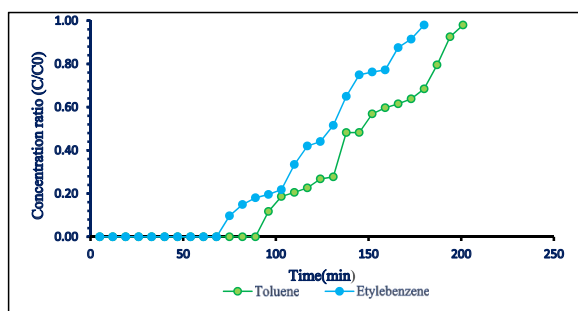| Pollutant	Adsorption capacity (mg/g)	Total adsorption percentage (%)	Time of breakthrough (min)	Time of equilibration (min)	LUB value
Toluene	218	20	90	200	2.2
Ethylbenzene	143	44	70	180	2.44

Fig. 11. Breakthrough cure of toluene and ethylbenzene co-adsorption on ZIF-67.

4. Conclusion and future prospects

This investigation has successfully showcased the utility of ZIF-67 as an effective adsorbent for volatile organic compounds (VOCs), focusing on its application within fixed-bed column systems for air purification. Furthermore, the study underscores the significance of adsorption technology in managing air pollutants that are present at low concentrations and pose substantial toxicity risks. Through a methodical approach, ZIF-67 was synthesized and characterized using various techniques. The BET surface area and total pore volume of ZIF-67 were 1578.7 m^2/g and 0.6 cm^3/g, respectively. As-synthesized ZIF-67 subsequently underwent thermal activation in both the air and nitrogen atmospheres. The comprehensive characterization of this material revealed its robust structure and suitability for VOC adsorption, particularly toluene.

Among the tested conditions, the ZIF-67$_{Air}$/250 °C sample emerged as the most proficient, demonstrating superior adsorption parameters. Its adsorption capacity, breakthrough time, and adsorption percentage were 414 mg/g, 420 min, and 77.7 %, respectively.

Operational factors such as relative humidity and toluene concentration were scrutinized to assess their impact on the performance of ZIF-67. It was observed that increased humidity led to a pronounced decline in all adsorption parameters, attributable to water molecules preferentially occupying active sites on the ZIF-67 surface. Therefore, increasing the RH from 30 % to 70 % decreases the adsorption capacity from 353.8 mg/g to 222.5 mg/g. Conversely, a reduction in toluene concentration in the influent stream from 1000 to 100 ppm resulted in a 41 % decrease in adsorption capacity but extended to 37 % in breakthrough time, indicating a trade-off between adsorption efficiency and duration of adsorbent performance. Therefore, The Yoon-Nelson, Yan, and Thomas models proved to be effective tools for simulating breakthrough curves, providing valuable insights into the adsorption dynamics of ZIF-67. The models' statistical parameters closely mirrored the empirical data, suggesting their potential for predictive application in real-world scenarios. The values of q$_y$ and q$_T$, derived from the Yan and Thomas model at 1000 ppm toluene, were determined to be 414.8 and 417.8 mg/g, respectively. Notably, these values closely align with the experimentally obtained adsorption capacity of 414.5 mg/g. The co-adsorption examination of toluene and ethylbenzene revealed a 65.6 % higher affinity of ZIF-67 for toluene adsorption. Additionally, a 98 % efficiency of the ZIF-67's regeneration reveals the reusability of the adsorbent and the recoverability of the adsorbate. While this study has laid a good foundation for the use of MOFs in VOC adsorption, several pathways for future research are identified:

1. Further research could explore the modification of MOFs with functional groups or composites to enhance their selectivity and capacity for specific VOCs.
2. The long-term viability of MOFs as adsorbents would be better understood through studies focused on their regeneration efficiency and the retention of adsorptive qualities over multiple cycles.
3. Life-cycle assessments of MOFs production and utilization could inform its environmental footprint and guide sustainable practices in its application.
4. Investigating other activation methods, such as microwave, vacuum, or chemical activation, may uncover more energy-efficient or effective ways to prepare MOFs for VOC adsorption.
5. The implementation of more sophisticated modelling techniques, including machine learning algorithms, could refine the prediction of adsorption behaviors under varying operational conditions.
6. Expanding the range of VOCs tested with MOFs, especially those with different chemical properties, could help in developing a more universal adsorbent material.
7. Field tests in real-world environments with fluctuating temperatures, humidity levels, and pollutant concentrations would validate the laboratory findings and enhance the material's readiness for commercial deployment.

By continuing to explore these avenues, the future of MOFs in VOC adsorption technology looks promising, potentially offering a robust and efficient solution to a pressing environmental challenge.

CRediT authorship contribution statement

Zabiholah Damiri: Supervision, Methodology, Investigation, Formal analysis. **Saeed Jafari:** Writing – original draft, Supervision, Project administration, Methodology, Investigation, Formal analysis, Conceptualization. **Saeed Yousefinejad:** Methodology, Investigation, Conceptualization. **Hossein Kazemian:** Writing – review & editing, Project administration, Methodology, Conceptualization.

Declaration of competing interest

The authors declare that they have no known competing financial interests or personal relationships that could have appeared to influence the work reported in this paper.

Acknowledgment

References

[1] X. Wang, et al., Benzene/toluene/water vapor adsorption and selectivity of novel C-PDA adsorbents with high uptakes of benzene and toluene, Chem. Eng. J. 335 (2018) 970–978, https://doi.org/10.1016/j.cej.2017.10.102.

[2] L. Rokni, et al., Effect of persistent organic pollutants on human health in South Korea: a review of the reported diseases, Sustainability 15 (14) (2023) 10851, https://doi.org/10.3390/su151410851.

[3] V.K. Gupta, N. Verma, Removal of volatile organic compounds by cryogenic condensation followed by adsorption, Chem. Eng. Sci. 57 (14) (2002) 2679–2696, https://doi.org/10.1016/S0009-2509(02)00158-6. %@ 0009-2509.

[4] X. Zhang, et al., Adsorption of VOCs onto engineered carbon materials: a review, J. Hazard Mater. 338 (2017) 102–123, https://doi.org/10.1016/j.jhazmat.2017.05.013.

[5] A. Aziz, K.S. Kim, Adsorptive volatile organic removal from air onto NaZSM-5 and HZSM-5: kinetic and equilibrium studies, Water, Air, Soil Pollut. 228 (9) (2017), https://doi.org/10.1007/s11270-017-3497-z.

[6] S.K. Lim, et al., Risk assessment of volatile organic compounds benzene, toluene, ethylbenzene, and xylene (BTEX) in consumer products, J. Toxicol. Environ. Health 77 (22–24) (2014) 1502–1521, https://doi.org/10.1080/15287394.2014.955905.

[7] L. Zhu, et al., A critical review on VOCs adsorption by different porous materials: species, mechanisms and modification methods, J. Hazard Mater. 389 (2020) 122102, https://doi.org/10.1016/j.jhazmat.2020.122102.

[8] L. Liu, et al., In situ fabrication of highly active γ-MnO2/SmMnO3 catalyst for deep catalytic oxidation of gaseous benzene, ethylbenzene, toluene, and o-xylene, J. Hazard Mater. 362 (2019) 178–186, https://doi.org/10.1016/j.jhazmat.2018.09.012.

[9] F.I. Khan, A.K. Ghoshal, Removal of volatile organic compounds from polluted air, J. Loss Prev. Process. Ind. 13 (6) (2000) 527–545, https://doi.org/10.1016/S0950-4230(00)00007-3. %@ 0950-4230.

[10] G. Gan, et al., Adsorption and membrane separation for removal and recovery of volatile organic compounds, J. Environ. Sci. (China) 123 (2023) 96–115, https://doi.org/10.1016/j.jes.2022.02.006.

[11] K.O. Iwuozor, et al., Do adsorbent pore size and specific surface area affect the kinetics of methyl orange aqueous phase adsorption? Journal of Chemistry Letters 2 (4) (2021) 188–198, https://doi.org/10.22034/jchemlett.2022.327407.1048. %@ 2821-0123.

[12] Y. Kong, et al., Enhanced tetracycline adsorption using alginate-graphene-ZIF67 aerogel, Colloids Surf. A Physicochem. Eng. Asp. 588 (2020), https://doi.org/10.1016/j.colsurfa.2019.124360.

[13] L. Zhu, et al., Metal-organic frameworks/carbon-based materials for environmental remediation: a state-of-the-art mini-review, J. Environ. Manag. 232 (2019) 964–977, https://doi.org/10.1016/j.jenvman.2018.12.004.

[14] P. Silva, et al., Multifunctional metal-organic frameworks: from academia to industrial applications, Chem. Soc. Rev. 44 (19) (2015) 6774–6803, https://doi.org/10.1039/C5CS00307E.

[15] X. Li, et al., Adsorption materials for volatile organic compounds (VOCs) and the key factors for VOCs adsorption process: a review, Separ. Purif. Technol. 235 (2020), https://doi.org/10.1016/j.seppur.2019.116213.

[16] S. Mazloomi, et al., Parametric study and process modeling for metronidazole removal by rhombic dodecahedron ZIF-67 crystals, Sci. Rep. 13 (1) (2023) 14654.

[17] A.A. Mohammadi, et al., Comparative removal of hazardous cationic dyes by MOF-5 and modified graphene oxide, Sci. Rep. 12 (1) (2022) 15314.

[18] A.A. Mohammadi, et al., Comparative removal of hazardous cationic dyes by MOF-5 and modified graphene oxide, Sci. Rep. 12 (1) (2022) 15314.

[19] M. Shams, et al., Tailoring the topology of ZIF-67 metal-organic frameworks (MOFs) adsorbents to capture humic acids, Ecotoxicol. Environ. Saf. 269 (2024) 115854, https://doi.org/10.1016/j.ecoenv.2023.115854.

[20] A. Omarova, et al., MOF-199-based coatings as SPME fiber for measurement of volatile organic compounds in air samples: optimization of in situ deposition parameters, Microchem. J. 185 (2023) 108263, https://doi.org/10.1016/j.microc.2022.108263.

[21] A. Omarova, et al., New in situ solvothermally synthesized metal-organic framework MOF-199 coating for solid-phase microextraction of volatile organic compounds from air samples, Microporous Mesoporous Mater. 328 (2021) 111493, https://doi.org/10.1016/j.micromeso.2021.111493.

[22] A. Omarova, et al., A review on preparation methods and applications of metal–organic framework-based solid-phase microextraction coatings, Microchem. J. 175 (2022) 107147, https://doi.org/10.1016/j.microc.2021.107147.

[23] K. Li, et al., Zeolitic imidazolate frameworks for kinetic separation of propane and propene, J. Am. Chem. Soc. 131 (30) (2009) 10368–10369, https://doi.org/10.1021/ja9039983.

[24] G. Zhong, et al., The application of ZIF-67 and its derivatives: adsorption, separation, electrochemistry and catalysts, J. Mater. Chem. A 6 (5) (2018) 1887–1899, https://doi.org/10.1039/C7TA08268A.

[25] B. Chen, et al., A cost-effective method for the synthesis of zeolitic imidazolate framework-8 materials from stoichiometric precursors via aqueous ammonia modulation at room temperature, Microporous Mesoporous Mater. 193 (2014) 7–14, https://doi.org/10.1016/j.micromeso.2014.03.006.

[26] C. Duan, et al., Recent progress on synthesis of ZIF-67-based materials and their application to heterogeneous catalysis, Green Energy Environ. 7 (1) (2022) 3–15, https://doi.org/10.1016/j.gee.2020.12.023.

[27] S. Jafari, et al., Effects of post-synthesis activation and relative humidity on adsorption performance of ZIF-8 for capturing toluene from a gas phase in a continuous mode, Appl. Sci. 8 (2) (2018) 310, https://doi.org/10.3390/app8020310.

[28] J. Qian, et al., Hydrothermal synthesis of zeolitic imidazolate framework-67 (ZIF-67) nanocrystals, Mater. Lett. 82 (2012) 220–223, https://doi.org/10.1016/j.matlet.2012.05.077.

[29] Y. Pan, et al., Adsorptive removal of phenol from aqueous solution with zeolitic imidazolate framework-67, J. Environ. Manag. 169 (2016) 167–173, https://doi.org/10.1016/j.jenvman.2015.12.030.

[30] Y. Liu, et al., Importance of surface modification of γ-alumina in creating its nanostructured composites with zeolitic imidazolate framework ZIF-67, J. Colloid Interface Sci. 526 (2018) 497–504, https://doi.org/10.1016/j.jcis.2018.05.008.

[31] H.S. Jhinjer, et al., Metal-organic frameworks functionalized smart textiles for adsorptive removal of hazardous aromatic pollutants from ambient air, J. Hazard Mater. 411 (2021) 125056, https://doi.org/10.1016/j.jhazmat.2021.125056.

[32] K. Vellingiri, et al., Metal-organic frameworks for the adsorption of gaseous toluene under ambient temperature and pressure, Chem. Eng. J. 307 (2017) 1116–1126, https://doi.org/10.1016/j.cej.2016.09.012.

[33] Y. Bian, et al., Metal–organic framework-based nanofiber filters for effective indoor air quality control, J. Mater. Chem. A 6 (32) (2018) 15807–15814, https://doi.org/10.1039/C8TA04539A.

[34] H. Patel, Fixed-bed column adsorption study: a comprehensive review, Appl. Water Sci. 9 (3) (2019) 45, https://doi.org/10.1007/s13201-019-0927-7.

[35] M. Suzuki, M. Suzuki, Adsorption Engineering, Kodansha, Tokyo, 1990.

[36] L.K. Wang, et al., Air Pollution Control Engineering, Springer, 2004.

[37] J.-H. Kim, et al., Sorption equilibrium and thermal regeneration of acetone and toluene vapors on an activated carbon, Ind. Eng. Chem. Res. 46 (13) (2007) 4584–4594, https://doi.org/10.1021/ie0609362.

[38] A.C. Fernandes, J. Pires, Adsorption of volatile organic compounds on zeolite L, J. Chem. Eng. Data 61 (11) (2016) 3890–3896, https://doi.org/10.1021/acs.jced.6b00624.

[39] S. Jafari, et al., Adsorptive removal of toluene and carbon tetrachloride from gas phase using Zeolitic Imidazolate Framework-8: effects of synthesis method, particle size, and pretreatment of the adsorbent, Microporous Mesoporous Mater. 268 (2018) 58–68, https://doi.org/10.1016/j.micromeso.2018.04.013.

[40] X. Zhang, et al., Enhanced adsorption performance of gaseous toluene on defective UiO-66 metal organic framework: equilibrium and kinetic studies, J. Hazard Mater. 365 (2019) 597–605, https://doi.org/10.1016/j.jhazmat.2018.11.049.

[41] X. Zhang, et al., Enhanced hydrophobic UiO-66 (University of Oslo 66) metal-organic framework with high capacity and selectivity for toluene capture from high humid air, J. Colloid Interface Sci. 539 (2019) 152–160, https://doi.org/10.1016/j.jcis.2018.12.056.

[42] K. Yang, et al., Adsorption of volatile organic compounds by metal-organic frameworks MOF-177, J. Environ. Chem. Eng. 1 (4) (2013) 713–718, https://doi.org/10.1016/j.jece.2013.07.005.

[43] S. Saghir, Z. Xiao, Synthesis of novel Ag@ ZIF-67 rhombic dodecahedron for enhanced adsorptive removal of antibiotic and organic dye, J. Mol. Liq. 328 (2021) 115323, https://doi.org/10.1016/j.molliq.2021.115323.

[44] S. Jafari, et al., Removal of toluene from air by zeolitic imidazolate framework-8: synthesis, characterization, and experimental breakthrough curve, Int. J. Sci. Stud. 5 (2017) 1073–1082, https://doi.org/10.17354/ijssI/2017/143. Curve.

[45] K.-J. Kim, H.-G. Ahn, The adsorption and desorption characteristics of a binary component system of toluene and methylethylketone on activated carbon modified with phosphoric acid, Carbon 48 (8) (2010) 2198–2202, https://doi.org/10.1016/j.carbon.2010.02.021.

[46] H.-B. Liu, et al., Enhanced adsorption of benzene vapor on granular activated carbon under humid conditions due to shifts in hydrophobicity and total micropore volume, J. Hazard Mater. 318 (2016) 425–432, https://doi.org/10.1016/j.jhazmat.2016.07.026.

[47] W.-T. Tsai, et al., Adsorption properties and breakthrough model of 1, 1-dichloro-1-fluoroethane on activated carbons, J. Hazard Mater. 69 (1) (1999) 53–66, https://doi.org/10.1016/S0304-3894(99)00058-8.

[48] G. Yan, et al., A new model for heavy metal removal in a biosorption column, Adsorpt. Sci. Technol. 19 (1) (2001) 25–43.

[49] L.c.F. Lima, et al., Fixed bed adsorption on benzene, toluene, and xylene (BTX) contaminants from monocomponent and multicomponent solutions using a commercial organoclay, Ind. Eng. Chem. Res. 56 (21) (2017) 6326–6336, https://doi.org/10.1021/acs.iecr.7b00173.

[50] X. Li, et al., Mechanistic insight into the interaction and adsorption of Cr (VI) with zeolitic imidazolate framework-67 microcrystals from aqueous solution, Chem. Eng. J. 274 (2015) 238–246, https://doi.org/10.1016/j.cej.2015.03.127.

[51] R. Banerjee, et al., High-throughput synthesis of zeolitic imidazolate frameworks and application to CO2 capture, Science 319 (5865) (2008) 939–943, https://doi.org/10.1126/science.1152516.

[52] R.P. Lively, et al., Ethanol and water adsorption in methanol-derived ZIF-71, Chem. Commun. 47 (30) (2011) 8667–8669, https://doi.org/10.1039/C1CC12728D;47(30):8667-9.

[53] V.F. Cheong, P.Y. Moh, Recent advancement in metal–organic framework: synthesis, activation, functionalisation, and bulk production, Mater. Sci. Technol. 34 (9) (2018) 1025–1045, https://doi.org/10.1080/02670836.2018.1468653.

[54] J.E. Mondloch, et al., Activation of metal–organic framework materials, CrystEngComm 15 (45) (2013) 9258–9264.

[55] X. Zhang, et al., A historical overview of the activation and porosity of metal–organic frameworks, Chem. Soc. Rev. 49 (20) (2020) 7406–7427, https://doi.org/10.1039/D0CS00997K.

[56] O.K. Farha, J.T. Hupp, Rational design, synthesis, purification, and activation of metal− organic framework materials, Accounts Chem. Res. 43 (8) (2010) 1166–1175, https://doi.org/10.1021/ar1000617.

[57] L.E. Mphuthi, et al., Synthesis and metal-exchange of nano-ZIF-67 with Ni (II) and Mn (II) for enhanced catalytic CO2 conversion, Mater. Today Commun. 34 (2023) 105458, https://doi.org/10.1016/j.mtcomm.2023.105458.

[58] Y. Li, et al., Synthesis of ZIF-8 and ZIF-67 using mixed-base and their dye adsorption, Microporous Mesoporous Mater. 234 (2016) 287–292, https://doi.org/10.1016/j.micromeso.2016.07.039.

[59] Z. Zhao, et al., Adsorption and diffusion of benzene on chromium-based metal organic framework MIL-101 synthesized by microwave irradiation, Ind. Eng. Chem. Res. 50 (4) (2011) 2254–2261, https://doi.org/10.1021/ie101414n.

[60] M. Bahri, et al., A comparative study on metal organic frameworks for indoor environment application: adsorption evaluation, Chem. Eng. J. 313 (2017) 711–723, https://doi.org/10.1016/j.cej.2016.10.004.

[61] Y. Li, et al., Mechanochemical synthesis of Cu-BTC@ GO with enhanced water stability and toluene adsorption capacity, Chem. Eng. J. 298 (2016) 191–197, https://doi.org/10.1016/j.cej.2016.03.141.

[62] H. Sui, et al., Application of silica gel in removing high concentrations toluene vapor by adsorption and desorption process, J. Taiwan Inst. Chem. Eng. 74 (2017) 218–224, https://doi.org/10.1016/j.jtice.2017.02.019.

[63] H. Brauer, Y.B. Varma, Air Pollution Control Equipment, Springer Science & Business Media, 2012.

[64] S. Hasan, et al., Agro-industrial waste 'wheat bran'for the biosorptive remediation of selenium through continuous up-flow fixed-bed column, J. Hazard Mater. 181 (1–3) (2010) 1134–1142, https://doi.org/10.1016/j.jhazmat.2010.05.133.

[65] L. Zhu, et al., A critical review on VOCs adsorption by different porous materials: species, mechanisms and modification methods, J. Hazard Mater. 389 (2020) 122102, https://doi.org/10.1016/j.jhazmat.2020.122102.

[66] S.-H. Pak, M.-J. Jeon, Y.-W. Jeon, Study of sulfuric acid treatment of activated carbon used to enhance mixed VOC removal, Int. Biodeterior. Biodegrad. 113 (2016) 195–200, https://doi.org/10.1016/j.ibiod.2016.04.019.